# Ion-beam-produced structural defects in ZnO

S. O. Kucheyev*
*Lawrence Livermore National Laboratory, Livermore, California 94550*

J. S. Williams and C. Jagadish
*Department of Electronic Materials Engineering, Research School of Physical Sciences and Engineering, The Australian National University, Canberra, ACT 0200, Australia*

J. Zou
*Australian Key Centre for Microscopy and Microanalysis, The University of Sydney, NSW 2006, Australia*

Cheryl Evans, A. J. Nelson, and A. V. Hamza
*Lawrence Livermore National Laboratory, Livermore, California 94550*
(Received 29 October 2002; revised manuscript received 15 January 2003; published 31 March 2003)

We study the evolution of lattice defects in single-crystal ZnO bombarded with 60-keV $^{28}$Si and 300-keV $^{197}$Au ions at 77 and 300 K. To characterize ion-beam-produced structural defects, we use a combination of Rutherford backscattering/channeling (RBS/C) spectrometry, cross-sectional transmission electron microscopy (XTEM), x-ray photoelectron spectroscopy, and atomic force microscopy. Results show that ZnO exhibits strong dynamic annealing, and even high-dose bombardment with heavy ($^{197}$Au) ions at 77 K does not render ZnO amorphous. However, a crystalline-to-amorphous phase transition can be induced by irradiation with relatively light $^{28}$Si ions. In this latter case, amorphization is attributed to strong chemical effects of Si atoms implanted into the ZnO lattice, resulting in the stabilization of an amorphous phase. High-dose heavy-ion bombardment also results in a strong stoichiometric imbalance (loss of O) in the near-surface region. A variation in irradiation temperature from 77 up to 300 K has a minor effect on the damage buildup behavior in ZnO bombarded with Au ions. Data analysis also shows that a variation in the density of collision cascades by increasing ion mass from $^{28}$Si up to $^{197}$Au has a negligible effect on the damage buildup behavior. For both light- ($^{28}$Si) and heavy- ($^{197}$Au) ion bombardment regimes, XTEM reveals that ion irradiation produces energetically favorable planar defects which are parallel to the basal plane of the wurtzite structure of ZnO. Interestingly, our RBS/C study also reveals the formation of a *middle defect peak* between the surface and bulk peaks of disorder in Au-implanted ZnO, but not in Si-bombarded samples. The formation of this middle peak, most likely to be related to complex defect agglomeration processes, is rather unexpected and, to our knowledge, has not been observed in any other material. Physical mechanisms of defect formation in ZnO under ion bombardment are discussed based on these experimental findings.

DOI: 10.1103/PhysRevB.67.094115 PACS number(s): 61.72.Cc, 61.72.Dd, 68.55.Ln, 61.72.Vv

## I. INTRODUCTION

Zinc oxide is a II-VI semiconductor with a room-temperature direct band gap of ~3.4 eV. At 300 K and atmospheric pressure, it has the wurtzite lattice structure. Current technological applications of polycrystalline ZnO ceramics and powders are numerous, and they have been extensively reviewed elsewhere.[1,2] In addition, over the past several decades, single-crystal ZnO has been considered as a potential candidate for a range of optoelectronic devices as well as devices for high-temperature/high-power electronics.[1–6] Problems with the growth of high-quality single crystals and problems associated with device processing have, however, hindered the advancement of single-crystal-ZnO-based (opto)electronics.

Recent tremendous success in the growth of large-area device-quality ZnO single crystals (both bulk and epilayers) (Refs. 4–7) has attracted considerable research effort to develop a device processing technology and to understand the properties of this material. However, at present, there are still serious challenges to overcome for processing ZnO, including electrical doping, metallization, and electrical isolation. In particular, even very early studies[1] have shown that a controllable doping (and, in particular, *p*-type doping) of ZnO is rather challenging due to the complex behavior of intrinsic lattice defects in this material.

Controllable selective-area electrical doping of ZnO can, in principle, be achieved by ion implantation. However, previous attempts to dope ZnO (in particular, with potential *p*-type dopants) by ion implantation have not been very successful.[8–10] The problem with doping by ion implantation is obviously related to dopant activation efficiency and undesirable effects of ion-beam-produced lattice defects on the electrical properties of the material. It is clear that an understanding of ion-beam-damage processes in ZnO, to be achieved via detailed studies, is highly desirable if the large potential of ion implantation as a device processing tool is to be fully exploited. Such systematic studies of ion-implanted ZnO are also obviously crucial for understanding the fundamental properties of lattice defects and impurities in this material.

Up to now, a number of studies have been reported on

 ©2003 The American Physical Society

structural,[11–23] optical,[9,13,24–33] electrical,[8,17,34–40] and magnetic[34,35,41] properties of single-crystal ZnO exposed to irradiation with energetic particles. It has been shown that ZnO exhibits strong dynamic annealing (i.e., migration and interaction of ion-beam-generated defects *during* ion irradiation) and remains crystalline even after bombardment to rather high doses of keV heavy ions.[12,18,19] For example, previous studies have shown that, under bombardment with 360-keV $^{208}$Pb ions (which generate dense collision cascades) at 77 K, the ZnO lattice does not exhibit an ion-beam-induced crystalline-to-amorphous transition even for extremely high ion doses (up to $10^{17}$ cm$^{-2}$) when each lattice atom has been ballistically displaced hundreds of times.[18] This situation arises because most Frenkel pairs (i.e., lattice vacancies and interstitials), ballistically generated in ZnO by the ion beam, experience annihilation, and only a very small portion of such migrating point defects avoids annihilation to agglomerate into energetically stable defect complexes. Such extremely efficient dynamic annealing of ion-beam-generated defects significantly complicates the damage accumulation behavior in ZnO, as will be discussed in more detail below.

It has also been shown that lattice defects produced in ZnO by high-dose bombardment with keV ions, studied by Rutherford backscattering/channeling (RBS/C) spectrometry, can largely (though not completely) be removed by thermal annealing at $\sim$1275 K.[19] This is somewhat surprising since it is most often observed that extended defects are only completely removed by annealing at approximately two-thirds of the melting temperature (in Kelvin).[42] Hence, one can expect that relatively large thermal budgets (with temperatures $\gtrsim$1500 K) will be necessary to anneal irradiation-produced defects in ZnO, given its melting point of $\sim$2250 K. This fact again points to an additional complexity in the behavior of ion-beam-produced defects in ZnO, not observed in many other semiconductors.

The above observations strongly suggest that systematic studies of the structural characteristics of ion-implanted ZnO are warranted. In particular, a number of technologically important (and, at the same time, physically interesting) issues of ion-beam processes in ZnO need to be studied in detail. These include (i) the damage buildup behavior, (ii) the defect microstructure, (iii) the effect of irradiation parameters (such as ion mass, energy, dose, implant temperature, and ion-beam flux), (iv) possible ion-beam-induced stoichiometric changes, and (v) chemical effects of implanted species (i.e., cases in which atomic species implanted into the lattice affect the damage buildup behavior and defect stability).

In this paper, we investigate the structural characteristics of ZnO bombarded with keV heavy ($^{197}$Au) and relatively light ($^{28}$Si) ions at room and liquid-nitrogen temperatures. Depth profiles of near-surface gross lattice disorder in the Zn sublattice are studied by RBS/C. Cross-sectional transmission-electron microscopy (XTEM) is applied to identify the structure of ion-beam-produced defects. In addition, we use x-ray photoelectron spectroscopy (XPS) to characterize the stoichiometry of implanted layers. Finally, ion-irradiation-produced changes in surface morphology are studied by atomic force microscopy (AFM). Our results reveal interesting features of the ion-beam-damaging behavior of ZnO. In particular, we show that keV heavy-ion ($^{197}$ Au) bombardment leads to significant stoichiometric disturbances in the ZnO lattice but does not induce a nonequilibrium crystalline-to-amorphous phase transformation even for the case of very large ion doses. However, such a crystalline-to-amorphous phase transition can be induced in ZnO by irradiation with much lighter $^{28}$Si ions. This can be attributed to strong chemical effects of the implanted Si atoms. Interestingly, our RBS/C study also reveals that heavy-ion bombardment of ZnO results in the formation of a *middle defect peak* between the surface and bulk peaks of disorder. Below, we present these experimental data and discuss physical mechanisms responsible for the observed behavior.

## II. EXPERIMENT

Single-crystal bulk wurtzite ZnO samples used in this study were purchased from Cermet, Incorporated. As specified by the grower, the samples were (0001) oriented, O face polished, and had an etch pit density of $<4\times10^4$ cm$^{-2}$. Samples were implanted with 300-keV $^{197}$Au$^+$ ions at 77 or 300 K with a beam flux of $\sim3\times10^{12}$ cm$^{-2}$ s$^{-1}$ over the dose range from $8\times10^{13}$ up to $4\times10^{16}$ cm$^{-2}$ with an ANU 1.7 MV tandem accelerator (NEC, 5SDH-4). Implantation with 60-keV $^{28}$Si$^-$ ions was done at 77 K with a beam flux of $\sim1.2\times10^{13}$ cm$^{-2}$ s$^{-1}$ over the dose range from $2\times10^{15}$ up to $8\times10^{16}$ cm$^{-2}$ with the ANU 180-kV ion implanter. During implantation, samples were tilted by $\sim7°$ relative to the incident ion beam to minimize channeling.

After implantation, all samples were characterized *ex situ* at room temperature by RBS/C using an ANU 1.7 MV tandem accelerator (NEC, 5SDH) with 1.8-MeV $^4$He$^+$ ions incident along the [0001] direction and backscattered into detectors at 98°, 115°, and $\sim$168° relative to the incident-beam direction. An 8° glancing-angle detector geometry was used to provide enhanced depth resolution for examining near-surface damage accumulation. Scattering geometries with larger glancing angles were used to separate Au and Zn peaks in RBS/C spectra in samples implanted up to high Au doses ($\geqslant5\times10^{15}$ cm$^{-2}$). All RBS/C spectra were analyzed using one of the conventional algorithms[43] for extracting depth profiles of the effective number of scattering centers. For brevity, the number of scattering centers, normalized to the atomic concentration, will be referred to below as ''relative disorder.''

To characterize the microstructure of ion-beam-produced lattice defects, selected samples were studied by XTEM in a Philips CM12 transmission-electron microscope operating at 120 kV. Specimens for XTEM were prepared by 3.5-keV Ar$^+$-ion-beam thinning using a Gatan precision ion-polishing system. The effect of ion bombardment on the surface morphology was studied by AFM under ambient conditions with a Nanoscope III scanning probe microscope.

Selected samples were also studied by XPS with a Quantum 2000 scanning XPS system with a focused monochromatic Al $K\alpha$ x-ray source (1486.7 eV) for excitation and a spherical section analyzer. An $\sim$20-$\mu$m diameter x-ray beam was incident normal to the sample surface, and the detector

was at 45° away from the normal. To study variations in the near-surface composition, ion-beam sputter etching was performed with a 2-keV $Ar^+$-ion beam tilted ~45° off the surface normal. Previous studies have shown that semiconductor films can often be sputtered with up to ~3-keV Ar ions without artificially changing the composition.[44]

Ballistic calculations presented in this paper were performed with the TRIM code[45] with a threshold displacement energy ($E_{th}$) of 57 eV for both Zn and O sublattices. Such a value of $E_{th}$ was chosen based on experimental data by Locker and Meese.[34,35] The values of displacements per atom (DPA) quoted here are the concentration of ion-beam-generated lattice vacancies normalized to the atomic concentration of ZnO.

It should be noted that, as discussed more fully elsewhere,[46–48] some thermal annealing of ion-beam-produced lattice defects may have occurred during warming the low-temperature-implanted samples up to room temperature before the subsequent RBS/C or XTEM analysis. Although we do not expect a pronounced thermal annealing of implantation disorder at 300 K due to extremely efficient dynamic annealing processes in ZnO,[48] this effect presently deserves additional experimental studies.

## III. RESULTS

In this section, we present experimental data on damage processes in ZnO bombarded with heavy ($^{197}$Au) and relatively light ($^{28}$Si) ions. Of interest in this study of the fundamental ion-beam-defect processes are the main features of the damage buildup behavior, ion-beam-induced phase transformations, types of irradiation-produced defects, implantation-induced stoichiometric imbalance, the effects of the density of collision cascades, and chemical effects of implanted atoms.

### A. Bombardment with $^{197}$Au ions

#### *1. Depth profiles of disorder*

Figure 1(a) shows RBS/C spectra illustrating the damage buildup in ZnO bombarded at 77 K with 300-keV Au ions. It is seen from Fig. 1(a) that the depth profiles of ion-beam-produced lattice defects are apparently bimodal. Indeed, Fig. 1(a) shows that, with increasing ion dose, lattice disorder in the Zn sublattice accumulates both in the crystal bulk and near the sample surface.[49] Such bimodal damage-depth profiles are not uncommon for ion-implanted semiconductors, for which disorder typically accumulates in the crystal bulk (where the nuclear energy-loss profile is maximum) and at the sample surface (which is often a sink for ion-beam-generated point defects).[48,50]

However, several notable features of RBS/C spectra from Fig. 1(a) deserve further attention. First, Fig. 1(a) shows that the apparent position of the bulk defect peak, which also depends on ion dose, is at ~500−800 Å. This depth is closer to the projected range of 300-keV Au ions (~500 Å) rather than to the maximum of the nuclear energy-loss profile of these ions (~320 Å), as calculated using the TRIM code.[45] We will come back to this fact in Sec. IV A, when discussing the mechanism of the damage buildup in ZnO.

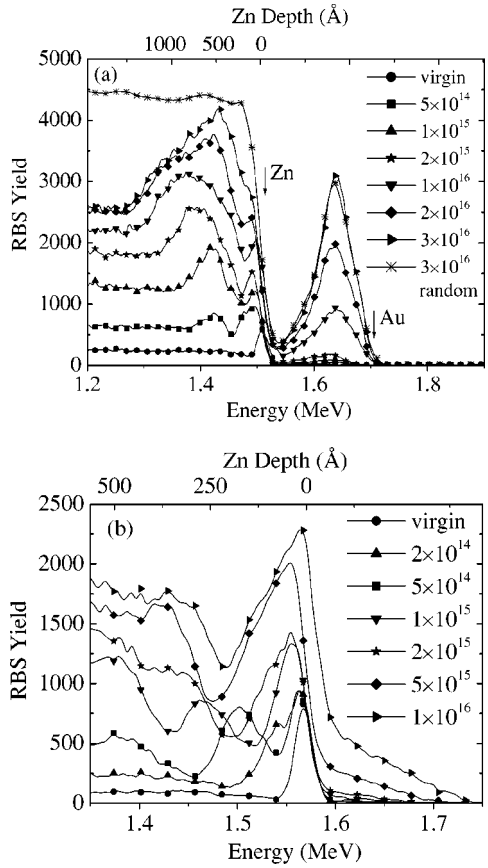


FIG. 1. Selected RBS/C spectra [acquired with 25° (a) and 8° (b) glancing-angle detector geometries] showing the damage buildup in the near-surface layer of ZnO bombarded at 77 K with 300-keV Au ions with a beam flux of $\sim 3\times 10^{12}$ cm$^{-2}$ s$^{-1}$. Implantation doses (in cm$^{-2}$) are indicated in the legend. The positions of the surface peaks of Au and Zn are denoted by arrows in (a). Note that the random spectrum in (a) is given for an ion dose of $3\times 10^{16}$ cm$^{-2}$, and the near-surface random yield in (b) corresponds to ~2800 counts. Also note that, for clarity, only every fourth (a) or sixth (b) experimental point is displayed in the spectra.

Figure 1(a) also reveals a shift of the position of the bulk defect peak to lower backscattering energies with increasing ion dose (and, hence, the level of lattice disorder). Such a shift can partly be attributed to the difference in the depth scales of random and aligned spectra (i.e., the difference in the energy loss of the analyzing He ions for random and channeling directions). This effect has been discussed in more detail elsewhere.[50,51] It should also be noted that the depth scales in the RBS/C spectra reported in the present paper have been calculated with the stopping powers of Zn and O in an amorphous matrix. Hence, such a depth scale should be more accurate for spectra with large damage levels, where error resulting from the different stopping power of channeled He ions should be small.

The ion dose dependence of the maximum relative disorder in the bulk defect peak [as extracted from RBS/C spectra such as those shown in Fig. 1(a)] is illustrated in Fig. 2(a) for ZnO bombarded with 300-keV Au ions at 77 or 300 K. It is

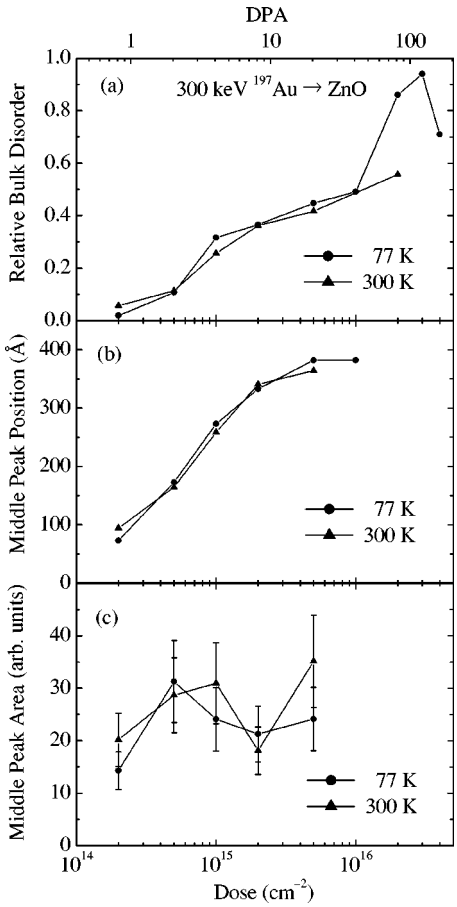


FIG. 2. Results of the analysis of RBS/C spectra acquired from ZnO bombarded at 77 and 300 K with 300-keV Au ions with a beam flux of $\sim 3\times 10^{12}$ cm$^{-2}$ s$^{-1}$. The ion dose dependence of the maximum relative disorder in the bulk defect peak is shown in (a). The position and area of the middle defect peak as a function of ion dose are illustrated in (b) and (c), respectively. The top scale gives the values of DPA at the depth of the maximum of the nuclear energy-loss profile of 300-keV Au ions.

seen from Fig. 2(a) that, for both room- and liquid-nitrogen temperature irradiation regimes, bulk disorder gradually increases with increasing ion dose. Interestingly, an increase in irradiation temperature from 77 to 300 K has a negligible effect on the disorder buildup in the crystal bulk for ion doses $\lesssim 10^{16}$ cm$^{-2}$. For the case of bombardment with 300-keV Au ions at 77 K to doses above $\sim 10^{16}$ cm$^{-2}$, Fig. 2(a) reveals a strong increase in the amount of relative disorder, as measured by RBS/C. However, such an increase in the level of ion-beam-produced lattice damage for very large ion doses can be attributed to ion-beam-induced material decomposition, as will be discussed in more detail below. It could also be expected that bombardment at 300 K to doses higher than those used in this study ($\leqslant 2\times 10^{16}$ cm$^{-2}$) will result in pronounced stoichiometric imbalance, significantly affecting the RBS/C yield.

### *2. Middle defect peak*

Another interesting feature of RBS/C spectra such as shown in Fig. 1(a) (acquired with a 25° glancing-angle detector geometry) is an unusually broad surface peak observed for ion doses $\lesssim 5\times 10^{14}$ cm$^{-2}$. Moreover, the shape of RBS/C spectra from Fig. 1(a) for ion doses $\lesssim 10^{16}$ cm$^{-2}$ suggests that an additional peak exists between the surface and the bulk defect peaks, but this additional peak is not well resolved, given the limited depth resolution. To clarify this issue, we have performed a RBS/C analysis with an 8° glancing-angle detector geometry, which gives improved depth resolution in the near-surface region. Results of such an analysis are illustrated in Fig. 1(b), showing that RBS/C spectra indeed have an additional peak between the expected surface and bulk defect peaks. Interestingly, Fig. 1(b) shows that the position of this *middle defect peak* (MDP) changes with increasing ion dose. This effect is better illustrated in Fig. 2(b), showing that, as ion bombardment proceeds, the MDP originates at the sample surface and moves toward the bulk defect peak. For relatively large ion doses ($0.5-1\times 10^{16}$ cm$^{-2}$), Fig. 2(b) shows that the position of the MDP appears to be independent of ion dose and equals $\sim 380$ Å. It is also seen from Fig. 2(b) that, for the sample temperatures studied (77 and 300 K), the behavior of the MDP is independent of irradiation temperature, within experimental error.

It is interesting that for a dose of $8\times 10^{13}$ cm$^{-2}$—the smallest Au dose used in the present study—RBS/C spectra for both 77- and 300-K bombardment regimes are essentially indistinguishable from spectra for virgin (i.e., unimplanted) samples. However, irradiation with Au ions at 77 or 300 K to a dose of $2\times 10^{14}$ cm$^{-2}$ results in the formation of a MDP overlapping with the surface defect peak, as can be clearly seen from Fig. 1(b). Additional studies in the low-dose regime are desirable to identify whether there exists a critical ion dose for the formation of the MDP.

The behavior of the MDP is further illustrated in Fig. 2(c), which shows the ion dose dependence of the area of the MDP for the case of bombardment at 77 or 300 K with 300-keV Au ions. Such a defect peak area has been estimated by fitting the depth profiles of relative disorder (extracted from RBS/C spectra) with three overlapping Gaussian curves for surface, middle, and (normal) bulk defect peaks, respectively. It is seen from Fig. 2(c) that, within experimental error, the area of the MDP is independent of ion dose for both room- and liquid-nitrogen temperature irradiation regimes.

It should also be noted that, in contrast to Fig. 1(a), Zn and Au peaks overlap in higher-resolution RBS/C spectra shown in Fig. 1(b). However, our detailed RBS/C analysis with different scattering geometries (namely, with 4°, 8°, 15°, 25°, and 78° glancing-angle detector geometries) shows that the middle peak is related to scattering from Zn atoms, not from a possible segregation of implanted Au atoms. The formation of this middle peak is rather unexpected and, to our knowledge, has not been observed in any other material. Indeed, typical depth profiles of ion-beam-produced lattice disorder in crystalline solids have a Gaussian shape with one maximum (in addition to the surface defect peak), reflecting the depth profile of atomic displacements ballistically generated by the ion beam. Possible physical mechanisms for the formation of such a MDP are discussed in detail in Sec. IV B.

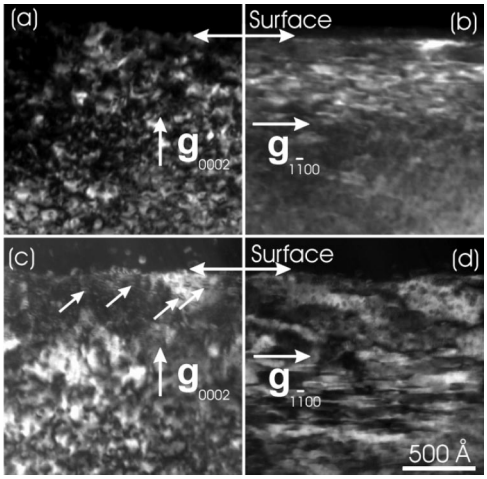


FIG. 3. Dark-field XTEM images [(a) and (c) $\mathbf{g}=0002^*$ and (b) and (d) $\mathbf{g}=1\bar{1}00^*$] of ZnO bombarded at 77 K with 300-keV Au ions with a beam flux of $\sim 3\times 10^{12}\,\mathrm{cm}^{-2}\,\mathrm{s}^{-1}$ to doses of $1\times 10^{15}$ [(a) and (b)] and $4\times 10^{16}\,\mathrm{cm}^{-2}$ [(c) and (d)]. All images are of the same magnification. Several precipitates are denoted by short arrows in (c).

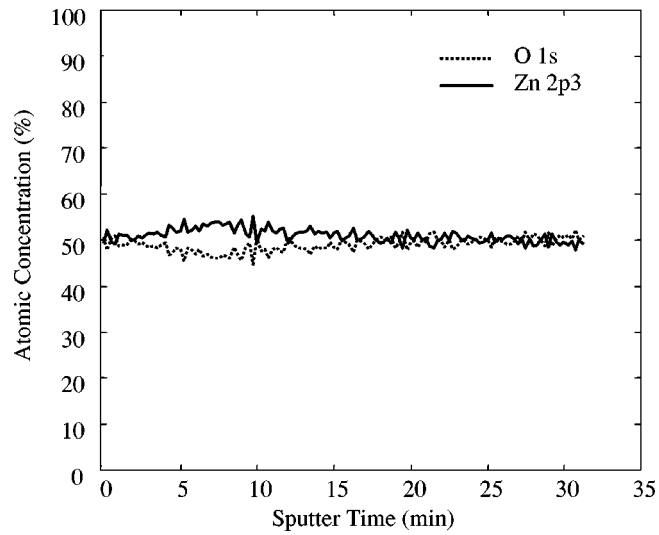


FIG. 4. XPS compositional depth profiles for ZnO implanted at 300 K with 300 keV Au ions to a dose of $2\times 10^{16}\,\mathrm{cm}^{-2}$ with a beam flux of $\sim 3\times 10^{12}\,\mathrm{cm}^{-2}\,\mathrm{s}^{-1}$. The sputter rate was $\sim 40$ Å/min.

#### *3. Defect microstructure*

Figure 3 shows dark-field XTEM images of ZnO bombarded at 77 K with 300-keV Au ions to doses of $1\times 10^{15}$ [Figs. 3(a) and 3(b)] and $4\times 10^{16}\,\mathrm{cm}^{-2}$ [Figs. 3(c) and 3(d)]. These (diffraction-contrast) images reveal the microstructure of ion-beam-produced defects consisting of some point defect clusters [see Figs. 3(a) and 3(c)] and coarse planar defects observed in $\mathbf{g}=1\bar{1}00^*$ images [see Figs. 3(b) and 3(d)].[52] These planar defects are parallel to the basal plane of the ZnO wurtzite structure. For a dose of $1\times 10^{15}\,\mathrm{cm}^{-2}$, a band of planar defects is observed in Fig. 3(b) in an $\sim$550-Å-thick near-surface layer. This depth is consistent with the damage-depth profile of lattice disorder studied by RBS/C and illustrated in Fig. 1. Interestingly, Fig. 3(d) reveals that, after a dose of $4\times 10^{16}\,\mathrm{cm}^{-2}$, this $\sim$550-Å-thick near-surface layer shows a different contrast, while a band of planar defects is observed at larger depths of $\sim 1100-1500$ Å for this ion dose. Also consistent with the RBS/C data discussed above, no amorphous phase is observed by XTEM in Fig. 3 even in a sample implanted at 77 K to a very high dose of $4\times 10^{16}\,\mathrm{cm}^{-2}$ of keV heavy ions. Figure 3(c) also reveals some precipitates ($\sim$50 Å in size) in a sample bombarded to a dose of $4\times 10^{16}\,\mathrm{cm}^{-2}$. These precipitates, denoted by arrows in Fig. 3(c), presumably consist of a Zn-enriched material as a result of ion-beam-induced material decomposition, which will be discussed more fully below. It should be also noted that ion-beam sputtering hinders studies of possible heavy-ion-induced lattice amorphization for larger ion doses. Indeed, doses of $10^{16}-10^{17}\,\mathrm{cm}^{-2}$ of heavy ions are within the sputter limit for ZnO, as has also been discussed previously.[18]

#### *4. Ion-beam-induced stoichiometric imbalance*

Variations in near-surface composition have further been studied by XPS. An XPS compositional depth profile for a virgin (i.e., as-grown) ZnO sample reveals good uniformity of Zn and O concentrations in the near-surface region characterized (i.e, in the first $\sim$1000 Å from the sample surface). Our data also show that bombardment at 300 K with 300-keV Au ions to a dose of $5\times 10^{14}\,\mathrm{cm}^{-2}$ does not result in any detectable stoichiometric imbalance. However, Fig. 4, showing the XPS compositional depth profiles for ZnO implanted at 300 K with 300-keV Au ions to a dose of $2\times 10^{16}\,\mathrm{cm}^{-2}$, reveals that irradiation to a larger ion dose ($2\times 10^{16}\,\mathrm{cm}^{-2}$) leads to pronounced loss of O near the sample surface. Hence, although high-dose bombardment with keV heavy ions does not induce a nonequilibrium crystalline-to-amorphous phase transition, such irradiation results in a relatively strong stoichiometric imbalance (loss of O). We come back to this effect in Sec. IV A.

### B. Bombardment with $^{28}$Si ions

#### *1. Depth profiles of disorder*

Figure 5 shows selected RBS/C spectra illustrating the evolution of lattice disorder in ZnO bombarded at 77 K with 60-keV Si ions. These RBS/C spectra reveal that, similar to the case of heavy-ion bombardment shown in Fig. 1, lattice disorder accumulates both at the surface and in the crystal bulk. In addition, the maximum of the bulk defect peak in Fig. 5 for ion doses $\gtrsim 10^{16}\,\mathrm{cm}^{-2}$ is close to the projected ion range ($\sim$525 Å) rather than to the maximum of the nuclear energy-loss profile ($\sim$300 Å). However, in contrast to the case of bombardment with 300-keV Au ions, no MDP is observed between surface and bulk peaks of disorder in this case of bombardment with relatively light $^{28}$Si ions. Figure 5 also shows that, for a dose of $5\times 10^{16}\,\mathrm{cm}^{-2}$, a buried amorphous layer appears to nucleate in the crystal bulk, as suggested by the RBS/C yield reaching the random level. Finally, irradiation with 60-keV Si ions to a dose of $8\times 10^{16}\,\mathrm{cm}^{-2}$ appears to amorphize the entire

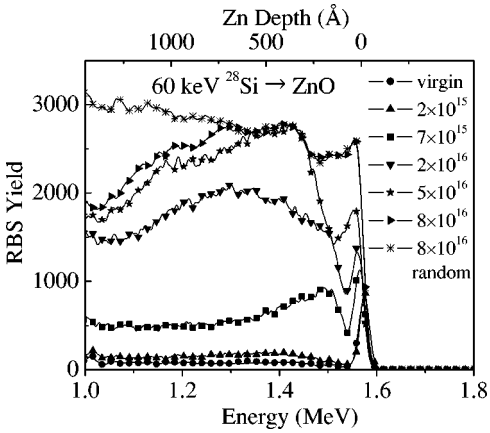


FIG. 5. Selected RBS/C spectra (acquired with an 8° glancing-angle detector geometry) showing the damage buildup in the near-surface layer of ZnO bombarded at 77 K with 60-keV Si ions with a beam flux of $\sim 1.2\times 10^{13}$ cm$^{-2}$ s$^{-1}$. Implantation doses (in cm$^{-2}$) are indicated in the legend. Note that the random spectrum is given for an ion dose of $8\times 10^{16}$ cm$^{-2}$. Also note that, for clarity, only every fourth experimental point is displayed in the spectra.

$\sim$700-Å-thick near-surface layer. Note that pronounced alternations (a dip and a shoulder) in the RBS/C random spectrum shown in Fig. 5 for a dose of $8\times 10^{16}$ cm$^{-2}$ is due to a large concentration of implanted Si atoms as well as possible diffusion of Si. Indeed, bombardment with 60-keV Si ions to a dose of $8\times 10^{16}$ cm$^{-2}$ results in the introduction of $\sim$15 at. % of Si atoms close to the projected ion range. Similar effects of high-dose light-ion implantation on RBS/C spectra have recently been discussed in detail in Refs. 48 and 50 for the case of another wide band-gap semiconductor, GaN.

The damage buildup behavior in ZnO bombarded with 60-keV Si ions is further illustrated in Fig. 6, showing the ion dose dependence of the maximum relative disorder in the bulk defect peak (as extracted from RBS/C spectra). It is seen from Fig. 6 that, for doses below $\sim 10^{16}$ cm$^{-2}$, the level of bulk disorder gradually increases with increasing ion dose. This damage buildup behavior is similar to that in the case of 300-keV Au-ion bombardment discussed above [see Fig. 2(a)]. However, for doses above $\sim 10^{16}$ cm$^{-2}$ of 60-keV Si ions, Fig. 6 reveals a rather fast buildup of lattice damage up to complete disordering, as measured by the ion channeling technique. Such a rapid disorder accumulation in the high-dose regime can be attributed to chemical effects of implanted Si ions, as is discussed in more detail in Sec. IV A.

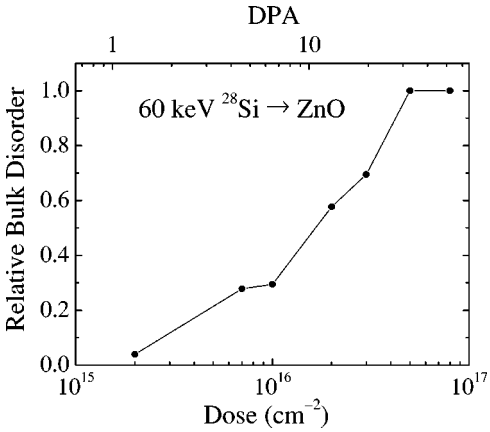


FIG. 6. Ion dose dependence of the maximum relative disorder in the bulk defect peak in ZnO samples bombarded at 77 K with 60-keV Si ions with a beam flux of $\sim 1.2\times 10^{13}$ cm$^{-2}$ s$^{-1}$.

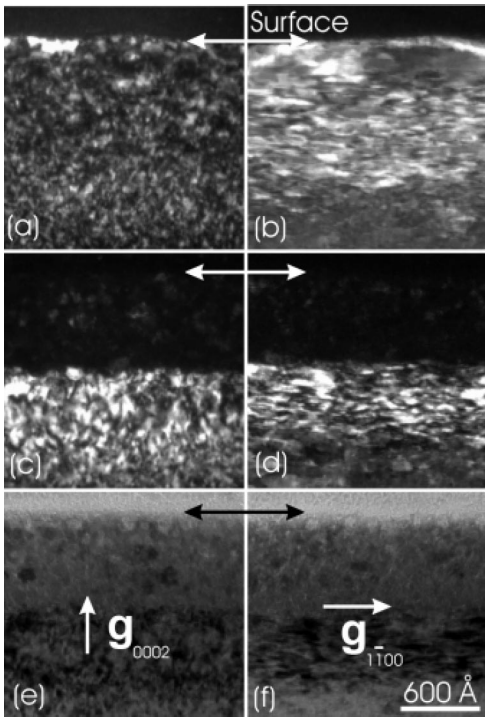


FIG. 7. Dark-field (a)–(d) and bright-field (e) and (f) XTEM images [(a), (c), and (e) **g**=0002* and (b), (d), and (f) **g** $=1\bar{1}00$*] of ZnO bombarded at 77 K with 60-keV Si ions with a beam flux of $\sim 1.2\times 10^{13}$ cm$^{-2}$ s$^{-1}$ to doses of $7\times 10^{15}$ [(a) and (b)] and $8\times 10^{16}$ cm$^{-2}$ [(c) – (f)]. All images are of the same magnification.

### *2. Defect microstructure*

To better understand the damage buildup behavior in ZnO implanted with Si ions, we have performed a XTEM study. Figure 7 shows XTEM images of ZnO bombarded at 77 K with 60-keV Si ions to doses of $7\times 10^{15}$ [Figs. 7(a) and 7(b)] and $8\times 10^{16}$ cm$^{-2}$ [Figs. 7(c)–7(f)]. Images from Figs. 7(a) and 7(b) show that irradiation to a dose of $7\times 10^{15}$ cm$^{-2}$ creates a dense band of point defect clusters and planar defects similar to those observed in Fig. 3 in the case of heavy-ion bombardment. Figure 7(b) also shows that, in the case of bombardment with 60-keV Si ions to a dose of $7\times 10^{15}$ cm$^{-2}$, the $\sim$300-Å-thick near-surface layer is essentially free from planar defects, which are concentrated in the deeper layer from $\sim$300 to $\sim$700 Å from the sample surface. This result is consistent with RBS/C data from Fig. 5, reflecting the depth profile of ion-beam-produced defects in this sample.

In the case of a sample implanted with 60-keV Si ions to a higher dose of $8\times 10^{16}$ cm$^{-2}$, Figs. 7(c)–7(f), as well as our selected-area diffraction analysis, confirm the amor-

phization of the ~725-Å-thick near-surface layer, as suggested by RBS/C data from Fig. 5. Amorphization can also be seen from a comparison of dark-field and bright-field XTEM images shown in Fig. 7. However, a close examination of Figs. 7(c) – 7(f) and electron-diffraction patterns reveals that amorphization is not complete, and some crystallites are clearly seen in both dark-field and bright-field images as bright and dark inclusions, respectively. This result is discussed in more detail in Sec. IV A.

## IV. DISCUSSION

In this section, we propose a scenario for defect processes in ZnO under ion bombardment. Special attention is given to possible physical mechanisms for the formation of the MDP observed in the present study in RBS/C spectra of ZnO bombarded with keV heavy ions.

### A. Damage buildup

Experimental data presented above show that single-crystal ZnO exhibits a high level of dynamic annealing. For example, Fig. 2(a) (see the top scale) shows that in order to reach a level of relative lattice disorder of ~0.6 during bombardment with 300-keV Au ions at 77 or 300 K, each lattice atom has to be ballistically displaced about one hundred times. The fact that single-crystal ZnO is highly resistant to ion-beam damaging indicates that primary defects generated by the ion beam are highly mobile at 77 K and above, and most of them experience effective annihilation. However, such effective defect annihilation is obviously not perfect, and the experiment shows that energetically favorable defect complexes accumulate in the ZnO lattice with increasing ion dose. Our (diffraction-contrast) XTEM studies of ZnO bombarded to relatively large doses of $^{28}$Si and $^{197}$Au ions (see Figs. 3 and 7) have revealed that such energetically favorable defect structures consist of point defect clusters and planar defects which are parallel to the basal plane of the ZnO wurtzite structure. It should be noted that a detailed XTEM study of the atomic structure of ion-beam-produced defects has not been possible in the present work due to a high density of implantation-produced defects. However, radiation defects have previously been studied by Yoshiie *et al.*[15,16] in ZnO irradiated with a (less damaging) electron beam in the transmission-electron microscope. These previous XTEM studies[15,16] have shown that high-energy (>700 keV) electron bombardment of ZnO at temperatures of 300–773 K results in the formation of dislocation loops which are interstitial in nature and have Burgers vectors of $1/2[0001]$ and $1/3\langle 11\bar{2}0\rangle$. It is plausible that similar dislocation loops form in ZnO as a result of dynamic annealing processes during keV light- or heavy-ion bombardment studied in the present work. However, verification of this possibility must await more detailed XTEM studies than those of the current work.

In this case of strong dynamic annealing during ion bombardment, the defect accumulation process is nucleation limited. This conclusion is supported by the fact that the apparent position of the bulk defect peak in both Si- and Au-implanted samples (see Figs. 1 and 5) is closer to the projected ion range rather than to the maximum of the nuclear energy-loss profile. Indeed, such a shift in the position of the bulk defect peak suggests that stable defect structures nucleate at the ion end of range stimulated by an excess of lattice interstitials and/or by the implanted Au or Si impurities. Such chemical effects of implanted species are particularly pronounced in the case of Si-implanted ZnO, where an ion-beam-induced crystalline-to-amorphous phase transition has been observed (Figs. 1 and 5). In addition, the effect of damage stabilization by implanted Si atoms can account for an asymmetric shape of RBS/C depth profiles in Fig. 5. A detailed (general) discussion of the physical mechanisms responsible for chemical effects of implanted species has previously been given in Ref. 48 and will not be reproduced here. It should be noted that, in the case of Si-implanted ZnO, amorphization is incomplete, with some crystallites imbedded into the amorphous matrix [see Figs. 7(c)–7(f)]. Such imperfect amorphization may be attributed to redistribution and segregation of Si atoms in the ZnO lattice during ion bombardment with the formation of localized regions enriched or depleted with Si.

Our results have also shown that, from 77 to 300 K, irradiation temperature has a negligible effect on the damage buildup behavior. This experimental fact suggests that, for 77–300 K, sample temperature has a minor effect on the stability of ion-beam-produced defect complexes and the efficiency of defect formation and annihilation processes. Such a negligible temperature effect may suggest an athermal mechanism for defect agglomeration and annihilation processes driven by electrostatic interaction between charged point defects whose formation is possible in ionic crystals. In this case, even very large dose heavy-ion bombardment at 77 K and above does not result in lattice amorphization, suggesting an instability of the amorphous phase in this temperature interval. Damage buildup and lattice amorphization studies at temperatures below 77 K would be desirable to better understand the influence of sample temperature on dynamic annealing processes and the stability of the amorphous phase in ZnO.

Previous detailed studies of ion-beam-damage processes in other semiconductor materials (see, for example, Refs. 48, 50, and 53, and references therein) have shown that the efficiency of the buildup of stable lattice defects under ion bombardment (at a given temperature) can strongly depend on the density of collision cascades. For example, it has previously been shown that, for GaN, both the level of ion-beam-produced stable lattice disorder (as measured by RBS/C) and the main features of the damage buildup behavior (such as surface vs bulk amorphization, saturation of the damage level in the crystal bulk, the sigmoidality of damage-dose curves, etc.) strongly depend on the density of collision cascades. Results of the present work allow us to study such an effect of collision cascade density in ZnO. Indeed, in the present study, we have used both relatively light 60-keV $^{28}$Si ions (which generate rather dilute collision cascades) and heavy 300-keV $^{197}$Au ions (which produced very dense collision cascades).

A comparison of Figs. 2(a) and 6 shows that the dependencies of relative bulk disorder on DPA [see the top scales

in Figs. 2(a) and 6] for Si- and Au-ion-bombardment regimes essentially overlap, within experimental error, for DPA values below $\sim 8$. This result indicates that a variation in the density of collision cascades by increasing ion mass from $^{28}$Si up to $^{197}$Au has a negligible effect on the damage buildup in ZnO. For DPA values above $\sim 8$ (corresponding to doses of 60-keV Si ions above $\sim 10^{16}$ cm$^{-2}$), Figs. 2(a) and 6 show that Si-ion bombardment results in a rapid increase in disorder, while the damage-DPA curves for the case of Au-ion bombardment exhibit a significantly smaller increase. However, in this high-dose regime, the buildup of lattice disorder under Si-ion bombardment is strongly affected by chemical effects of the implanted Si atoms, as discussed above.

It should also be noted that the fact that the buildup of lattice disorder in ZnO is essentially independent of the density of collision cascades is consistent with previous studies of the electrical properties of ZnO irradiated with MeV light ions (which generate rather dilute collision cascades).[40] As shown in Ref. 40, the ion doses necessary for electrical isolation of ZnO inversely depend on the number of lattice displacements produced by the ion beam, suggesting a negligible effect of collision cascade density on changes in electrical properties in the case of MeV light-ion bombardment. Results of the present study show that cascade density has also a negligible effect on the buildup of structural defects under keV ion bombardment.

### B. Middle defect peak

As alluded to earlier, the present study has revealed the formation of a MDP between the bulk and surface defect peaks in RBS/C spectra for heavy-ion-implanted ZnO. The formation of this middle peak is rather unexpected and, to our knowledge, has not been previously observed in any other material. Hence, we discuss this effect in more detail below. We first summarize the main experimental observations on the formation of the MDP and follow with a discussion of possible physical mechanisms responsible for its formation.

#### *1. Summary of experimental observations*

We can summarize the main experimental observations on the formation of the MDP as follows.

(i) The MDP is observed only for ZnO bombarded with keV heavy ions (300-keV $^{197}$Au ions), not for the case of bombardment with lighter 60-keV $^{28}$Si ions.

(ii) The MDP is observed for both room- and liquid-nitrogen temperature bombardment regimes, with a negligible effect of irradiation temperature varied from 77 to 300 K.

(iii) The MDP is related to the scattering of the analyzing He ions from Zn lattice atoms, not from a possible segregation of implanted Au atoms.

(iv) The MDP starts from the surface and moves deeper into the crystal bulk with increasing ion dose. The depth position of the MDP appears to be close to that of the bulk defect peak (independent of ion dose) for high ion doses [see Fig. 2(b)].

(v) The effective area of the MDP seems to be independent of ion dose.

#### *2. Possible physical mechanisms for the peak formation*

Below, we consider possible physical mechanisms for the formation of the MDP.

*a. Surface morphology.* The MDP can be caused by ion-beam-induced changes in surface morphology. However, our AFM study has not revealed any notable modification of the surface morphology as a result of ion bombardment in samples for which a pronounced MDP has been observed in RBS/C measurements. Hence, this mechanism is not supported by experimental data.

*b. Stoichiometric imbalance.* The MDP can also be due to ion-beam-induced stoichiometric imbalance. Indeed, our results (see Fig. 4) show that high-dose irradiation with 300-keV Au ions causes preferential loss of O in the near-surface region. One can assume that the MDP is a result of the scattering of channeling He ions from a border between O-deficient and stoichiometric regions of the material. Such a border is expected to move deeper into the crystal with increasing ion dose (and, hence, the width of the O-deficient region), which is consistent with the behavior of the MDP experimentally observed. However, as discussed in Sec. III A 4, our XPS study has revealed negligible stoichiometric changes in a sample bombarded at 300 K with 300-keV Au ions to a dose of $5\times 10^{14}$ cm$^{-2}$, while such bombardment causes the formation of a large and well-defined MDP (see Fig. 2). Hence, ion-beam-induced stoichiometric imbalance does not appear to be the main physical mechanism for the formation of the MDP.

*c. Band of defects.* The above discussion essentially rules out the possibility that the MDP in RBS/C spectra is related to measurement artifacts such as segregation of Au, large surface nonuniformities, or pronounced ion-beam-induced stoichiometric changes. This suggests that the mechanism for MDP formation is disorder related. For example, the MDP can be caused by the formation of a localized band of lattice defects resulting from imperfect defect annihilation processes during ion bombardment. A possible nucleation site for such a defect cluster formation, giving rise to a direct scattering peak in RBS/C spectra, can be an excess of ion-beam-generated lattice vacancies near the sample surface. Indeed, it is well known that vacancies and interstitials are spatially separated in a collision cascade, with an interstitial excess at the ion end of range and a vacancy excess closer to the surface.[54] This effect is expected to be pronounced for bombardment regimes with strong dynamic annealing,[50] which is the case for ZnO at least at liquid-nitrogen temperature and above. The importance of such a ballistic separation of interstitials and vacancies in the damage buildup behavior in ZnO bombarded with $^{197}$Au ions is also supported by the fact that the bulk defect peak is shifted, relative to the maximum of the nuclear energy-loss profile, closer to the ion end of range, the region with an interstitial excess (see the discussion in Sec. IV A).

This scenario for a defect-related formation of the MDP appears to be consistent with the experimental observations

summarized above. The fact that the MDP is observed only in ZnO samples bombarded with (heavy) $^{197}$Au ions (and not in samples irradiated with lighter $^{28}$Si ions) may suggest that the nucleation of the defect band giving rise to the MDP requires a large vacancy excess and the formation of dense collision cascades generated by heavy ions. The fact that the MDP moves deeper into the crystal bulk, with increasing ion dose, can be associated with the onset of ion-beam-induced loss of O from the sample surface as ion irradiation proceeds. Loss of O can stimulate defect annihilation processes in the region between the sample surface and the defect band giving rise to the MDP. Indeed, such O loss has been measured for higher ion doses when ion-beam-induced stoichiometric changes become significant (see Fig. 4). However, this intriguing dose dependence of the MDP position [Fig. 2(b)] can also be attributed to a possible increased defect annihilation at the sample surface. Additional work is presently needed to clarify the role of the sample surface and material stoichiometry in the formation and evolution of the MDP.

It should also be noted that, although our XTEM study has not revealed any sharp defect bands (see Fig. 3) at depths corresponding to the position of the MDP in RBS/C spectra in Au-ion-implanted ZnO, this observation does not rule out a defect-related mechanism for the formation of the MDP. Indeed, RBS/C and XTEM techniques are sensitive to different defect structures. The MDP is a direct-scattering peak, indicating that there are extra Zn atoms blocking the [0001] channels in the wurtzite lattice. As shown in Fig. 3, XTEM images of samples for which RBS/C reveals a strong MDP exhibit a dense stress-induced contrast caused by a large concentration of ion-beam-produced defects in the entire near-surface region implanted. The sensitivity of XTEM to a localized band of extra defects, giving rise to a direct-scattering peak in RBS/C spectra, may be poor due to such a large ''background'' concentration of ion-beam-produced lattice defects. Hence, XTEM results do not contradict the defect-related mechanism for the formation of the MDP. However, it is clear that additional studies are currently needed to fully understand this rather unusual and intriguing effect observed in ion-bombarded ZnO.

### C. Comparison with other materials

Finally, it is instructive to make a brief comparison of ion-beam-induced defect processes in ZnO, studied in this work, with those in other crystalline materials. Of particular interest for such a comparison are ion-beam-damage processes in another wurtzite wide band-gap semiconductor, GaN, studied in detail previously.[42] A rather detailed comparison of the damage buildup behavior in GaN with that in other semiconductors as well as metals has previously been given in Refs. 42, 48, and 50.

Results of previous[42,48,50] and present studies show that both materials (ZnO and GaN) exhibit strong dynamic annealing. This behavior is typical for materials with a large degree of ionicity.[12,57,58] However, a comparison of damage buildup curves from Figs. 2(a) and 6 with data from Refs. 48 and 50 indicates that ZnO is even more resistive to ion-beam-induced damaging than GaN. Moreover, ZnO does not exhibit the effect of defect saturation in the crystal bulk which has previously been observed in GaN.[48,50,55,56] The surface of ZnO is also not a nucleation site for amorphization, as it is in GaN. Indeed, for a wide range of ion-bombardment conditions, with increasing ion dose, amorphization of GaN proceeds layer by layer from the sample surface into the crystal bulk. In the case of ZnO, amorphization nucleates at the ion end of range, mediated by chemical effects of implanted Si atoms. Furthermore, in contrast to the case of GaN, the present study has revealed a negligible effect of the density of collision cascades on the damage buildup behavior in ZnO. However, both these materials exhibit ion-beam-induced stoichiometric imbalance as a result of high-dose heavy-ion bombardment, and, in both cases, implanted species can dramatically change the behavior of damage accumulation and stabilize an amorphous phase. Moreover, in both GaN and ZnO, defect structures resultant from imperfect dynamic annealing processes include planar defects parallel to the basal plane of the wurtzite lattice structure. Wang *et al.*[59] have recently performed a detailed XTEM study of such planar defects in ion-implanted GaN and found that these defects are interstitial in nature and have Burgers vectors of either $1/2[0001]$ or $1/6\langle 2\bar{2}03\rangle$ for a wide range of irradiation conditions.[60] Similar high-resolution XTEM studies are highly desirable to identify the nature of structural defects in ion-implanted ZnO.

## V. SUMMARY

In conclusion, we have studied the evolution of structural defects in ZnO bombarded with 60-keV Si or 300-keV Au ions. The main results of this work can be summarized as follows.

(i) At 77 K and above, ZnO exhibits very strong dynamic annealing and remains crystalline (though heavily damaged) even after a very high dose of heavy-ion bombardment.

(ii) High-dose ($\sim 10^{16}$ cm$^{-2}$) bombardment with 300-keV Au ions results in pronounced stoichiometric imbalance with preferential loss of O in the near-surface region.

(iii) A nonequilibrium crystalline-to-amorphous phase transition can be induced by bombardment with relatively light $^{28}$Si ions. In this case, an amorphous phase is effectively stabilized by implanted Si atoms.

(iv) A variation in irradiation temperature from 77 to 300 K has a minor effect on the damage buildup behavior and, hence, on the stability of ion-beam-produced defect complexes and the efficiency of defect formation and annihilation processes in this temperature interval.

(v) A variation in the density of collision cascades by increasing ion mass from $^{28}$Si up to $^{197}$Au has a negligible effect on the damage buildup behavior in ZnO.

(vi) Energetically favorable planar defects parallel to the basal plane of the wurtzite structure of ZnO are formed during both Si- and Au-ion irradiation regimes.

(vii) The formation of a middle defect peak between the surface and bulk peaks of disorder in Au-bombarded ZnO has been observed. Several physical mechanisms have been proposed for the formation of such a middle defect peak. At

this stage, the most plausible explanation appears to be disorder related. However, more work is presently needed to fully understand the formation of the middle defect peak in ion-bombarded ZnO.

(viii) Finally, a comparison of ion-beam-defect processes in ZnO with those in GaN have been made, showing that both materials exhibit strong dynamic annealing with a complex damage buildup behavior, typical for crystals with a large degree of ionicity of the chemical bonds.

**ACKNOWLEDGMENTS**

This research was supported in part by the Australian Research Council. Work at Lawrence Livermore National Laboratory was performed under the auspices of the U.S. Department of Energy by the University of California, Lawrence Livermore National Laboratory, under Contract No. W-7405-Eng-48.

*Email address: kucheyev1@llnl.gov

[1] W. Hirschwald, B. Bonasewicz, L. Ernst, M. Grade, D. Hofmann, S. Krebs, R. Littbarski, G. Neumann, M. Grunze, D. Kolb, and H. J. Schulz, Curr. Top. Mater. Sci. **7**, 143 (1981).
[2] D. R. Clarke, J. Am. Chem. Soc. **82**, 485 (1999).
[3] V. A. Nikitenko, Zh. Prikl. Spektrosk. **57**, 367 (1992).
[4] J. E. Nause, III-Vs Rev. **12**, 28 (1999).
[5] Y. Chen, D. Bagnall, and T. Yao, Mater. Sci. Eng., B **75**, 190 (2000).
[6] D. C. Look, Mater. Sci. Eng., B **80**, 383 (2001).
[7] K. Koike, T. Tanite, S. Sasa, M. Inoue, and M. Yano, Mater. Res. Soc. Symp. Proc. **692**, H11.9 (2002).
[8] B. W. Thomas and D. Walsh, J. Phys. D **6**, 612 (1973).
[9] B. J. Pierce and R. L. Hengehold, J. Appl. Phys. **47**, 644 (1976).
[10] S. O. Kucheyev, C. Jagadish, and J. S. Williams (unpublished).
[11] A. Ladage, Z. Phys. **144**, 354 (1956).
[12] H. M. Naguib and R. Kelly, Radiat. Eff. **25**, 1 (1975).
[13] D. Walsh, Solid-State Electron. **20**, 813 (1977).
[14] T. Yoshiie, H. Iwanaga, N. Shibata, M. Ichihara, and S. Takeuchi, Philos. Mag. A **40**, 297 (1979).
[15] T. Yoshiie, H. Iwanaga, N. Shibata, and S. Takeuchi, Philos. Mag. A **41**, 935 (1980).
[16] T. Yoshiie, H. Iwanaga, N. Shibata, K. Suzuki, M. Ichihara, and S. Takeuchi, Philos. Mag. A **47**, 315 (1983).
[17] E. Sonder, R. A. Zuhr, and J. R. Martinelli, Mater. Res. Soc. Symp. Proc. **60**, 365 (1986).
[18] C. W. White, L. A. Boatner, P. S. Sklad, C. J. McHargue, S. J. Pennycook, M. J. Aziz, G. C. Farlow, and J. Rankin, Mater. Res. Soc. Symp. Proc. **74**, 357 (1987).
[19] E. Sonder, R. A. Zuhr, and R. E. Valiga, J. Appl. Phys. **64**, 1140 (1988).
[20] J.-J. Couderc, J.-J. Demai, G. Vanderschaeve, and A. Peigney, Microsc. Microanal. Microstruct. **6**, 229 (1995).
[21] N. Tomiyama, M. Takenaka, and E. Kuramoto, Mater. Sci. Forum **105–110**, 1281 (1992).
[22] W. Puff, S. Brunner, P. Mascher, and A. G. Balogh, Mater. Sci. Forum **196–201**, 333 (1995).
[23] S. Brunner, W. Puff, P. Mascher, and A. G. Balogh, Mater. Res. Soc. Symp. Proc. **540**, 207 (1999).
[24] W. E. Vehse, W. A. Sibley, F. J. Keller, and Y. Chen, Phys. Rev. **167**, 828 (1968).
[25] I. Munder, R. Helbig, and J. Lagois, Solid State Commun. **41**, 553 (1982).
[26] M. Schilling, R. Helbig, and G. Pensl, J. Lumin. **33**, 201 (1985).
[27] J. Piqueras and E. Kubalek, Phys. Status Solidi A **91**, 569 (1985).
[28] G. Pazionis and H.-J. Schulz, Mater. Sci. Forum **10–12**, 839 (1986).
[29] J. A. Garcia, A. Remon, and J. Piqueras, Appl. Phys. A: Solids Surf. **42**, 297 (1987).
[30] V. P. Regel', V. A. Nikitenko, I. P. Kuzmina, V. G. Galstyan, T. P. Dolukhanyan, S. F. Nikul'shin, N. L. Sizova, and V. A. Skuratov, Zh. Tekh. Fiz. 57, 306 (1987) [Sov. Phys. Tech. Phys. **32**, 183 (1987)].
[31] V. A. Nikitenko, A. I. Tereshchenko, V. P. Kucheruk, K. E. Tarkpea, and I. P. Kuzmina, Inorg. Chem. **25**, 1425 (1990).
[32] V. A. Nikitenko, S. V. Mukhin, I. P. Kuzmina, and V. G. Galstyan, Inorg. Mater. (Transl. of Neorg. Mater.) **30**, 963 (1994).
[33] F. P. Denisov, V. A. Nikitenko, and I. P. Kuzmina, Radiat. Meas. **25**, 117 (1995).
[34] J. M. Meese and D. R. Locker, Solid State Commun. **11**, 1547 (1972).
[35] D. R. Locker and J. M. Meese, IEEE Trans. Nucl. Sci. **19**, 237 (1972).
[36] D. C. Look, J. W. Hemsky, and J. R. Sizelove, Phys. Rev. Lett. **82**, 2552 (1999).
[37] D. C. Look, D. C. Reynolds, J. W. Hemsky, R. L. Jones, and J. R. Sizelove, Appl. Phys. Lett. **75**, 811 (1999).
[38] F. D. Auret, S. A. Goodman, M. Hayes, M. J. Legodi, H. A. van Laarhoven, and D. C. Look, Appl. Phys. Lett. **79**, 3074 (2001).
[39] F. D. Auret, S. A. Goodman, M. Hayes, M. J. Legodi, H. A. van Laarhoven, and D. C. Look, J. Phys.: Condens. Matter **13**, 8989 (2001).
[40] S. O. Kucheyev, P. N. K. Deenapanray, C. Jagadish, J. S. Williams, M. Yano, K. Koike, S. Sasa, M. Inoue, and K. Ogata, Appl. Phys. Lett. **81**, 3350 (2002); S. O. Kucheyev, C. Jagadish, J. S. Williams, P. N. K. Deenapanray, M. Yano, K. Koike, S. Sasa, M. Inoue, and K. Ogata, J. Appl. Phys. **93**, 2972 (2003).
[41] J. M. Smithand W. E. Vehse, Phys. Lett. **31A**, 147 (1970).
[42] See, for example, a recent review by S. O. Kucheyev, J. S. Williams, and S. J. Pearton, Mater. Sci. Eng., R. **33**, 51 (2001).
[43] K. Schmid, Radiat. Eff. **17**, 201 (1973).
[44] See, for example, P. Corvini, A. Kahn, and S. Wagner, J. Appl. Phys. **57**, 2967 (1985).
[45] J. P. Biersack and L. G. Haggmark, Nucl. Instrum. Methods **174**, 257 (1980).
[46] W. Jiang, W. J. Weber, S. Thevuthasan, and D. E. McCready, J. Nucl. Mater. **257**, 295 (1998).
[47] W. J. Weber, W. Jiang, and S. Thevuthasan, Nucl. Instrum. Methods Phys. Res. B **166–167**, 410 (2000).
[48] S. O. Kucheyev, J. S. Williams, C. Jagadish, J. Zou, G. Li, and A. I. Titov, Phys. Rev. B **64**, 035202 (2001).
[49] A large peak around ~1.65 MeV is also seen in RBS/C spectra in Fig. 1(a). This peak is due to implanted Au atoms. These Au profiles, measured by RBS/C, follow expected Gaussian-like distributions predicted by ballistic calculations [such as the TRIM

code (Ref. 45)] and will not be further discussed in the present paper.

[50] S. O. Kucheyev, J. S. Williams, C. Jagadish, J. Zou, and G. Li, Phys. Rev. B **62**, 7510 (2000).

[51] J. S. Williams, M. Conway, J. A. Davies, M. Petravic, H. H. Tan, and J. Wong-Leung, Nucl. Instrum. Methods Phys. Res. B **136–138**, 453 (1998).

[52] It should be noted that irregular contrast observed in both implanted and unimplanted regions in **g**=0002* images presented in this paper can be attributed to lattice defects introduced into the near-surface region of a XTEM sample during the ion-beam thinning process. The absence of such an ion-beam-milling-induced contrast in other semiconductors (such as Si, Ge, GaAs, and GaN) can be attributed to the fact that, in these latter materials, bombardment with low-keV Ar ions, used for ion-beam milling, results in the amorphization of the near-surface layer. In contrast, the ZnO lattice remains crystalline (though heavily damaged) after bombardment with keV Ar ions, resulting in a strong defect-induced diffraction contrast experimentally observed.

[53] S. O. Kucheyev, J. S. Williams, J. Zou, G. Li, C. Jagadish, and A. I. Titov, Nucl. Instrum. Methods Phys. Res. B **190**, 782 (2002).

[54] See, for example, M. Nastasi, J. W. Mayer, and J. K. Hirvonen, *Ion-Solid Interactions: Fundamentals and Applications* (Cambridge University, Cambridge, England, 1996).

[55] W. Jiang, W. J. Weber, S. Thevuthasan, G. J. Exarhos, and B. J. Bozlee, MRS Internet J. Nitride Semicond. Res. **4S1**, G6.15 (1999).

[56] W. Jiang, W. J. Weber, and S. Thevuthasan, J. Appl. Phys. **87**, 7671 (2000).

[57] Based on calculations of Phillips (Ref. 58) ionicities of ZnO and GaN are 0.616 and 0.500, respectively.

[58] J. C. Phillips, *Bonds and Bands in Semiconductors* (Academic, New York, 1973).

[59] Y. G. Wang, J. Zou, S. O. Kucheyev, J. S. Williams, C. Jagadish, and G. Li, Electrochem. Solid-State Lett. **6**, G34 (2003).

[60] In addition, a detailed XTEM study of defect structures in GaN bombarded at 300 K with 600-keV $^{16}$O ions was recently reported by C. M. Yang, W. Jiang, W. J. Weber, and L. E. Thomas, J. Mater. Res. **17**, 2945 (2002).